

Operational machine learning for remote spectroscopic detection of CH₄ point sources

Vít Růžička^{a,b,d,*}, Gonzalo Mateo-García^b, Itziar Irakulís-Loitxate^{b,c}, Juan Emmanuel Johnson^b, Manuel Montesino San Martín^b, Anna Allen^b, Luis Guanter^c, David R. Thompson^d

^aUniversity of Oxford, Oxford, UK

^bInternational Methane Emissions Observatory, United Nations Environment Programme (UNEP),

^cUniversitat Politècnica de València (UPV), València, Spain

^dJet Propulsion Laboratory, California Institute of Technology, Pasadena, CA, USA

Abstract

Mitigating anthropogenic methane sources is one of the most cost-effective levers to slow down global warming. While satellite-based imaging spectrometers, such as EMIT, PRISMA, and EnMAP, can detect these point sources, current methane retrieval methods based on matched filters still produce a high number of false detections requiring laborious manual verification. This paper describes the operational deployment of a machine learning system for detecting methane emissions within the Methane Alert and Response System (MARS) of the United Nations Environment Programme's International Methane Emissions Observatory. We created the largest and most diverse global dataset of annotated methane plumes from three imaging spectrometer missions and quantitatively compared different deep learning model configurations. Focusing on the requirements for operational deployment, we extended prior evaluation methodologies from small tiled datasets to full granule evaluation. This revealed that deep learning models still produce a large number of false detections, a problem we address with model ensembling, which reduced false detections by over 74%. Deployed in the MARS pipeline, our system processes scenes and proposes plumes to analysts, accelerating the detection and analysis process. During seven months of operational deployment, it facilitated the verification of 1,351 distinct methane leaks, resulting in 479 stakeholder notifications. We further demonstrate the model's utility in verifying mitigation success through case studies in Libya, Argentina, Oman, and Azerbaijan. Our work represents a critical step towards a global AI-assisted methane leak detection system, which is required to process the dramatically higher data volumes expected from new and current imaging spectrometers.

Keywords: Methane, Artificial Intelligence, Deep Learning, Imaging spectroscopy, Hyperspectral data, Operational deployment, Benchmarking

1. Introduction

The reduction of anthropogenic methane emissions represents a critical component of global climate mitigation strategies. As the second largest contributor to global warming after CO₂ (Kuylenstierna et al., 2021), methane's short atmospheric lifetime makes its reduction a high-priority lever for achieving the climate targets outlined in the Intergovernmental Panel on Climate Change (IPCC) (Lee et al., 2023).

A key initiative of the United Nations Environmental Programme (UNEP) International Methane Emissions Observatory (IMEO) is the Methane Alert and Response System (MARS), which detects large point sources of methane emissions using satellite data. MARS utilizes a diverse array of imagery from various public space missions to identify plumes, notify stakeholders, and monitor sources globally over time. This initiative leverages both multispectral and hyperspectral satellite data. Although multispectral sensors offer higher data frequency and longer historical archives, they have limitations over heterogeneous landscapes such as dark, vegetated, or urban areas (Varon

et al., 2020; Gorroño et al., 2023). In contrast, hyperspectral sensors provide the enhanced sensitivity required to detect smaller emissions, even across the most complex surfaces (Irakulís-Loitxate et al., 2022; Guanter et al., 2021; Roger et al., 2024).

The current landscape of hyperspectral remote sensing missions includes a diverse and growing array of data sources. These include airborne hyperspectral sensors, such as NASA's AVIRIS series and EDF's MethaneAIR; instruments hosted on the International Space Station (ISS), such as NASA's EMIT; and a host of satellite missions, including DLR's EnMAP, ASI's PRISMA, EDF's MethaneSAT, the Chinese Gaofen (GF-5) and Ziyuan (ZY-1) series, and the recently launched Tanager-1 mission from Carbon Mapper and Planet. Furthermore, this collection of sensors is expected to expand significantly, with several next-generation methane-sensitive satellites under development, such as NASA's SBG (estimated to generate 10x more data than EMIT) and Carbon-I, ESA's CHIME, or DLR's CO2Image.

The increasing volume of data from current and forthcoming hyperspectral missions requires the automation of methane emission detection. Existing detection workflows, which are

*Corresponding author

Email address: ruzicka@jpl.nasa.gov (Vít Růžička)

based on labour intensive manual review, are inefficient for systematically monitoring large areas and are only suited to monitoring and studying previously identified emission sources. Consequently, a critical need exists for automated tools that can support analysts in monitoring not only known sites but also in discovering new emission events over vast geographical regions. Furthermore, automation can systematize the otherwise arduous and subjective task of delineating the geographic extent of methane plumes, which is a critical step for quantifying emission rates that currently depends on inconsistent human interpretation.

This paper describes a fully operational methane plume detection system integrated into MARS at UNEP’s IMEO. By automating the initial screening of hyperspectral satellite data, the models developed in this study facilitate the systematic monitoring of vast areas and the discovery of previously unknown emitters. This capability substantially reduces the manual workload for analysts, allowing a small team to efficiently process a global data stream. In the operational workflow, the system flags candidate plumes for subsequent manual verification, which ensures the correctness and identifies relevant stakeholders for notification (United Nations Environment Programme, 2024). The integration of this model into the MARS pipeline enhances operational efficiency by enabling timely detection of emission events for rapid stakeholder engagement and by scaling monitoring capabilities to support a more comprehensive and systematic analysis of methane dynamics and regulatory accountability.

Operationalizing a robust and scalable machine learning system for this task required significant advances beyond prior research. Our key contributions are: (i) the curation and public release of the largest and most diverse global dataset of manually annotated methane plumes, compiled from three distinct hyperspectral missions; (ii) a rigorous evaluation of various model configurations and a comprehensive performance analysis on full satellite granules, culminating in an ensemble approach that reduces false alerts by over 74% compared to the prior state-of-the-art (Růžička et al., 2023); (iii) the demonstration of successful zero-shot generalisation across sensors, with models trained on EMIT data evaluated on PRISMA and EnMAP, whose performance is further enhanced with fine-tuning; (iv) the successful integration of our models into the UNEP IMEO’s MARS operational pipeline, where it processed almost 20,000 scenes, resulting in 1,351 verified methane leaks, and 479 stakeholder notifications over the first five months of operation of the model; and (v) a demonstration of the model’s utility not only for initial detection but also for the verifying successful mitigation, substantiated by case-studies in Libya, Argentina, Oman, and Azerbaijan.

The remainder of the paper is organized as follows: Section 2 reviews the literature on methane detection and prior machine learning approaches. Section 3 describes the datasets from the EMIT, PRISMA, and EnMAP missions. Section 4 details our machine learning methodology and Section 5 outlines our experimental setup for both single-sensor training and cross-sensor adaptation. Section 6 presents our findings on model performance, false positive reduction, operational deployment

results, and mitigation case-studies. Finally, Section 7 offers concluding remarks and discusses future work.

2. Background literature

Here, we briefly review prior work using machine learning models for methane detection. For a more in-depth review, we refer the reader to surveys such as (Tiemann et al., 2024) or the background chapters of (Růžička, 2025).

Early scientific papers of (Frankenberg et al., 2016; Thompson et al., 2016; Duren et al., 2019; Irakulis-Loitxate et al., 2021, 2022) systematically explore large selected geographical regions and demonstrate that methane leaks can be tracked with both multispectral (MSI) (Varon et al., 2020; Sánchez-García et al., 2021; Irakulis-Loitxate et al., 2022) and hyperspectral (HSI) (Duren et al., 2019; Irakulis-Loitxate et al., 2021; Guntner et al., 2021; Roger et al., 2024) instruments. These articles measure methane enhancement using band ratios for MSI data (Varon et al., 2020) and matched filter approaches for HSI data (Thompson et al., 2015), but the identification of discrete point sources remains mostly manual.

Soon after, the first automated approaches leveraging machine learning models trained on either raw (Joyce et al., 2023) or interpreted satellite data followed (Jongaramrungruang et al., 2022; Groshenry et al., 2022). As highlighted by the opinion piece of (Thompson and Brodrick, 2021), research in developing machine learning models for hyperspectral data has been limited by the availability of large, annotated datasets. As such, these early works either considered only a relatively small numbers of real methane leak events, or they depend on simulation of synthetic data. Some of the first large, annotated datasets were presented by NASA in the work of (Cusworth et al., 2021) using aerial campaign of AVIRIS-NG over the Permian Basin region in the US. In the works of (Růžička et al., 2023; Kumar et al., 2023), this data has enabled training more complex machine learning models on real methane leak events.

Furthermore, (Růžička et al., 2023) have cleared and refined the ground truth labels from this dataset and released the data in a machine learning ready format. They also showcased some early examples of generalisation across sensors, by detecting events in data from the spaceborne instrument EMIT. The recent work of (Mancoridis et al., 2025b) further explores cross sensors adaptation using generative machine learning models.

Worth noting is also the work exploring different ways of computing methane enhancement products. The most widely used approaches derive from the matched filter method (Thompson et al., 2015), for example its iterative variant called Mag1c (Foote et al., 2020b). More recently, variants using extended spectral ranges of imaging spectroscopy data were proposed as the wide-window matched filter in (Roger et al., 2023). A similar approach is also noted in (Bue et al., 2025) as the full VSWIR variant of the column-wise matched filter (full CMF). We however note that most of these works do not quantitatively compare these methane enhancement products on large datasets.

Additionally, some of the very recent research, such as (Růžička and Markham, 2025) explores end-to-end process-

ing of imaging spectroscopy data without needing to compute the matched filter product (and instead directly using radiance cubes as input). However, these approaches require adapting traditional machine learning architectures to handle the large number of input bands.

Only few of the recent works consider true operational settings and potential deployment of the machine learning models. The work of (Vaughan et al., 2024b), demonstrates detection of methane leaks in selected monitoring locations using multispectral Sentinel-2 and Landsat imagery with refined version of the models proposed in (Vaughan et al., 2023). These models are currently used in the UNEP’s operational methane plume detection pipeline for multispectral data processing. The recent preprint of (Bue et al., 2025), developed at a similar time as our paper, considers using machine learning models as part of the detection pipeline at NASA. At the time of this writing, these models are not yet deployed.

Finally, we highlight that none of the prior published works have used a dataset of methane leak events in hyperspectral data as large as the one we are releasing in this paper (including 3 different sensors). Our comparative study of different methane enhancement products is also novel at this scale. As far as we know, our machine learning models are also the first operationally deployed and daily used models for detecting methane leaks in hyperspectral data enabling event discovery in novel regions.

In this paper we present datasets created from three hyperspectral sensors. We compute several methane enhancement products from this data and use them to train machine learning models from recent research (Růžička et al., 2023). We explore several additions to these models, such as using wind and location as additional inputs. Finally, we report results on realistic test sets created to mirror the production environment, namely in using the entire captured image (the full tile). We identify shortcomings of existing models and explore the usage of model ensembles to address these limitations.

3. Data

The datasets used in this paper originate from the operational archive of the UNEP IMEO’s Methane Alert and Response System (MARS), containing validated emission events from September 2022 to March 2025. Within this framework, a team of analysts identified a large number of methane leaks across various sectors and geographic areas, annotating each with high-quality semantic segmentation outlines. A key feature of this dataset is its rigorous validation: every detection was verified by at least two independent analysts, with a third confirmation required for any plume notified to stakeholders. This work leverages these verified detections from three hyperspectral sensors: EMIT (Green, 2022), PRISMA (Cogliati et al., 2021), and EnMAP (Storch et al., 2023). The global coverage of the resulting datasets is visualized in Figure 2.

3.1. EMIT dataset

The EMIT dataset currently forms the largest released dataset of methane leak events from a hyperspectral sensor with global

coverage. EMIT is an imaging spectrometer deployed on the ISS, which provides a near-global coverage of Earth since its launch in July 2022. The mission has been extended at least until 2026. EMIT captures images with ground resolution of 60 m, with spectral bands between 381 nm and 2493 nm, and spectral resolution of approximately 7.5 nm. The sensor produces images of about 76.8 km x 74.52 km area. We refer to these as *full tile* or *full granule* captures.

We create our dataset from 3806 methane leak events detected by the IMEO team. Figure 1 details the stratification of these events into sectors and countries. An additional 5965 locations that have been validated as not containing any plume leaks are included in this dataset. In total the dataset uses 3917 unique EMIT captures, 1528 of which contain plumes. These sources add up to more than 7.8 Tb of data, so extracting small tiles from these full scenes is necessary to reduce the size. Specifically, we extract smaller subregions of 256x256px (about 15.36 x 15.36 km) as geotiff files to reduce data storage requirements. These tiles are centered around methane leak events, so further tiling is suggested to break this regularity. It is important to bookkeep which tiles overlap so that they can be kept in same validation splits. To this end, we split tiles into train, validation and test subsets using selected date ranges, which ensures that different splits do not use the same source scene. These splits are shown on Figure 3. For training they are further tiled and augmented according to the input resolution of the models. A selected sample of data from the test split, 105 plume events and 95 no-plume images, are also downloaded as full EMIT tiles.

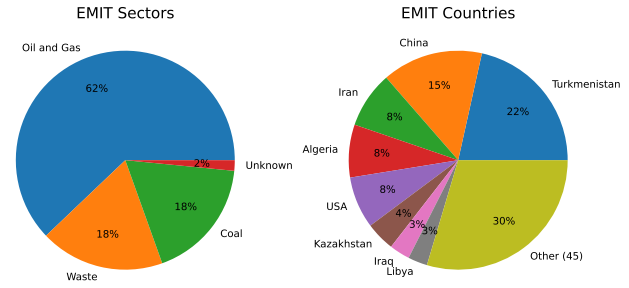
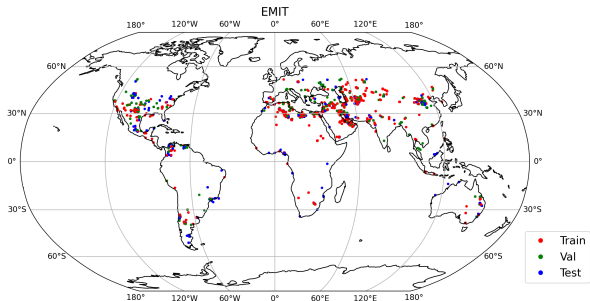


Figure 1: Stratification of EMIT data by sectors and countries.

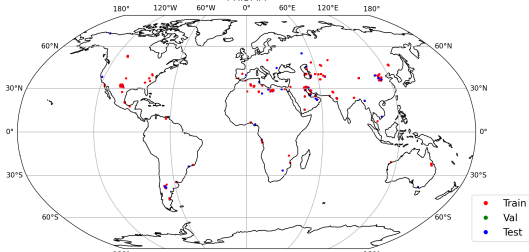
3.2. PRISMA and EnMAP datasets

We create two other datasets from the hyperspectral sensors PRISMA and EnMAP. In contrast to the larger EMIT dataset, we choose to use spatial rather than temporal data splits.

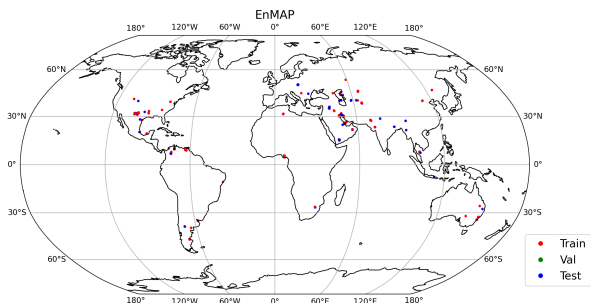
As these satellites operate in on-demand mode (whereas EMIT captures all ground based overpassed locations), the number of methane leak events is smaller - this highlights the fact that manual scheduling of satellite targets misses many events that may only be found later in the globally collected data archive. This allows us to explore a general multi-sensor scenario, where we have a very large dataset from a single sensor and smaller datasets from other sensors. This will be a typical situation for newly deployed sensors that have observed only few methane leak events.



(a) EMIT



(b) PRISMA



(c) EnMAP

Figure 2: Spatial distribution of samples in the created datasets and their division into train (red), validation (green, only for EMIT) and test (blue) subsets.

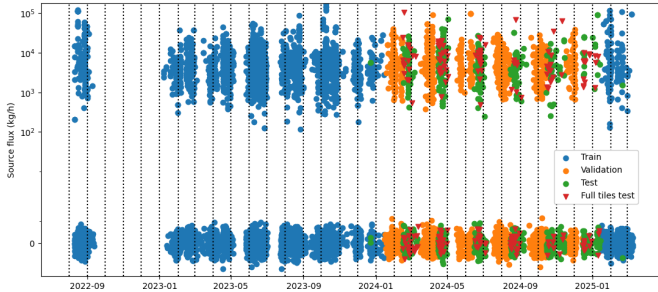


Figure 3: Temporal distribution of samples in the EMIT dataset. Training, validation and test subsets are also shown, full tiles are downloaded for selected samples from the test subset. Note that for no plume tiles (with fluxrate equal to 0), we jitter these points around x-axis for better visualisation.

The PRISMA dataset consists of 466 plume events and 664 selected no-plume locations. The PRISMA sensor observes spectral bands between 400 and 2505 nm, with spectral reso-

lution of approximately 11-13 nm and ground resolution of 30 m. We extract tiles of 256x256 px and split them into spatially non-overlapping train and test subsets. For the entire test set, we download the full sensor data of 115 images with in total 63 methane leak events and 52 background scenes.

The EnMAP dataset is the smallest, consisting of 239 plume events and 320 no-plume locations. The EnMAP sensor has spectral bands between 420 and 2450 nm with spectral resolution of 6.5 nm and ground resolution of 30 m. As for the other datasets, we extract tiles of 256x256 px and split them into spatially non-overlapping train and test subsets. The entire test set includes 83 full tile images which contain 54 methane leak events and 29 background scenes.

For all datasets, we also include the wind information from the U₁₀ NASA GEOS-FP reanalysis product of (Molod et al., 2012).

Detailed statistics about the datasets and the created data splits are in Table 1.

Table 1: Overview of datasets created in this paper. Images refer to the 256x256 px tiles extracted from the full images, except for the samples in the full tile test sets, which are kept in their original resolution. Sites refer to unique locations. Meanwhile the number of original granules refers to the total number of separate satellite captures and can be used to compare the scale of these datasets with other sources. We note that during training the train splits are further tiled into smaller resolution (128x128 px with 64 px overlap and several augmentations).

MARS-EMIT dataset

Split	Images	Sites	Original granules
Train	5746	1590	2250
Val	2316	1244	954
Test	1709	1103	713
Full tile test	200	-	200

MARS-PRISMA dataset

Split	Images	Sites	Original granules
Train	904	467	342
Test	226	192	115
Full tile test	115	-	115

MARS-EnMAP dataset

Split	Images	Sites	Original granules
Train	391	293	156
Test	168	151	83
Full tile test	83	-	83

We split each sensor’s data into non-overlapping subsets. For our largest dataset of EMIT images, we create three splits (train, validation and test) using temporally non-overlapping date ranges. Specifically, we reserve all data from 2024 for the test and validation datasets. This allows us to use any images collected before (data starting from September 2022) and after for training. Thus, any future data collected by the EMIT sensor can be added to the training dataset for later iterations of

these models. Note that the ISS hosted sensor EMIT exhibits different coverage in summer and winter months. In order to provide representative subsets in both test and validation data, we divide data by the 15th of each month and assign data ranges beginning with odd months for the validation dataset (e.g.: 15th Jan to 15th Feb, not including the last day) and even months to the test dataset (e.g.: 15th Feb to 15th Mar, not including last day). The last date range (15th Dec 2024 to 15th Jan 2025) is kept in the test dataset. This split is visualised on Figure 3 and can be exactly reproduced using our released code (which will be made available upon publication and link will be added here).

In the case of PRISMA and EnMAP datasets, we instead follow spatially non-overlapping splits. This decision was made because the datasets are smaller, and a temporal data split might introduce unwanted overfitting in some locations. These locations are shown on Figure 2.

3.3. Methane enhancement products

An established practice for detection of methane leak events in hyperspectral data uses the so-called methane enhancement products (generally the estimates of methane concentration above background levels). These are classical target detection products computed from the source hyperspectral data. One such family of methods uses the matched filter (MF) operator. Matched filters are used to search for target spectral signatures in hyperspectral data. In the context of methane leak detection, we use a methane signature calculated from HITRAN absorption coefficients (Brown et al., 2013).

Matched filter products therefore reduce the hyperspectral datacube into a single band of information representing the enhancement of methane above the background level. These enhancement maps can then be used by trained specialists or by machine learning models. These products include several error sources, including instrument noise, but also artifacts from surface materials that are spectrally similar to methane. These so-called confounders typically include artificial structures such as roads and solar panels, as well as natural features such as mountain ranges or dunes in the desert.

Several variants of matched filter products were proposed to reduce these confounder effects. The algorithm called Mag1c (Foote et al., 2020a) proposes iterative re-computation of matched filters and adjusting of parameters for background estimation. The recently proposed wide-window matched filter (WMF) (Roger et al., 2023) instead uses a wider spectral range of source hyperspectral data to better represent the background of the scene. More concretely, we use the product referred to as MF SWIR by (Roger et al., 2023) computed from the following extended spectral ranges in EMIT data: 976.9nm - 1260nm and the full 1330nm - 2441.1nm.

Figure 4 shows an example visualisation of the three methane enhancement products. In our work, we compute all these matched filter products for all samples in the considered datasets. This enables us to compare methods using any of these classical products.

4. Methods

4.1. Machine learning models

In this paper, we use machine learning architectures based on the HyperSTARCOP models proposed by (Růžička et al., 2023). However, we explore modifications of these models with additional input information and we explore their use in production environments. The machine learning model uses the U-Net architecture (Ronneberger et al., 2015) with the MobileNet-v3 (Howard et al., 2019) network as the encoder. As inputs, we primarily use a combination of RGB bands and one of the selected matched filter products - MF, Mag1c or WMF. We also explore encoding the wind and location information as additional input bands. This is motivated by the practice established by the works of (Lang et al., 2023; Vaughan et al., 2024a). The model and its input products are illustrated in Figure 5.

As was initially explored in the work of (Růžička et al., 2023), models trained on matched filter products can generalise on data across sensors. In this unique situation of using three datasets from three distinct hyperspectral sensors, we explore zero-shot generalisation and fine-tuning techniques. Specifically, we explore if models trained on the largest dataset of events in EMIT can aid in the detection of methane leaks also in data from the other two sensors.

Finally, we explore the robustness of the proposed machine learning models for their deployment in production pipelines. For this, we extend the evaluation of the models to full granules rather than restricting them to the small chips in the test set. These constitute what is referred to as in-the-wild data in the domain of Computer Vision. In-the-wild data typically has a different distribution and balance of classes than the training set, with many more negative cases. This can induce a very large number of false positive detections. In order to reduce the number of false positive detections in full tiles, we use model ensembles. For reporting results, it is custom to train the same machine learning model with several repetitions each with differently initialised weights, this is used to report average and standard deviation of the scores. Here, we can however treat these repeatedly trained models as an ensemble. Model ensembles have been used to improve prediction capabilities, and also in uncertainty estimation literature such as (Beluch et al., 2018; Růžička et al., 2020). Intuitively, different models in the ensemble will have learned different internal representations of the data that are all compatible with a limited training dataset. When presented with a new, potentially out-of-distribution sample, they will provide different predictions on uncertain data. Using the average output of the ensemble has a regularizing influence, reducing the impact of initial weights on the prediction outcome. The suggestion to use model ensembles for improved methane leak detection has been outlined as one of the potential future research directions in (Růžička, 2025).

4.2. Matched filter thresholding baselines

As baseline methods, we use thresholding of the various methane enhancement products followed by morphological operations to reduce the so-called salt-and-pepper noise in predic-

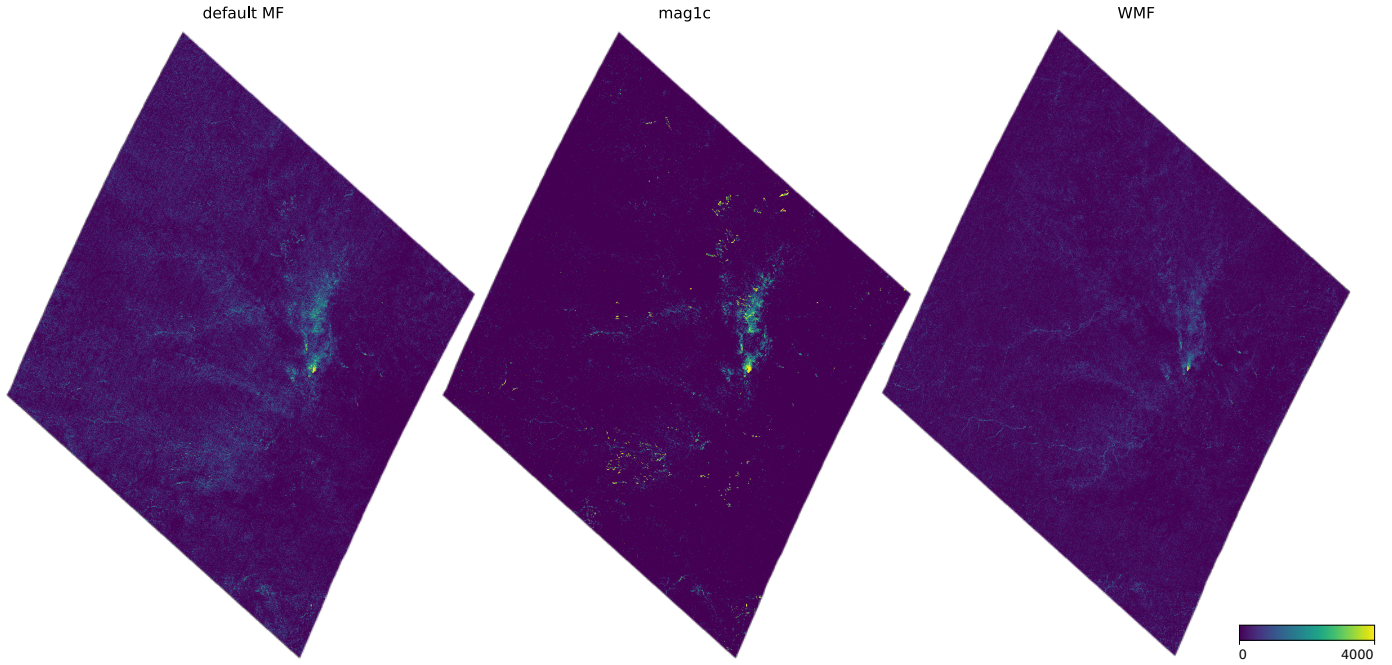


Figure 4: Comparison of the explored methane enhancement products computed for a sample scene from the EMIT full tile test split. For easier comparison, all matched filter products were scaled to the same visualisation range (0 to 4000 ppm·m units corresponding to the mixing ratio length). While some artifacts copy the structure of the real scene (e.g. rivers and mountain ranges) in all products, the Mag1c product seems to have most prominent confounders.

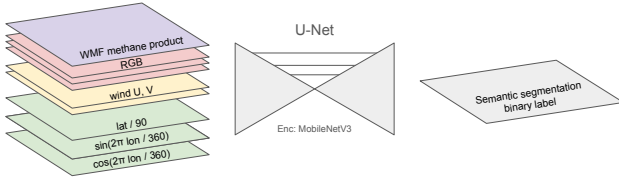


Figure 5: HyperMARS model illustration. We use the U-Net model architecture with the MobileNetV3 encoder and a variety of input features further described in the text. Depending on the used configuration of input products, the model has around 6.69M trainable parameters.

tions. The same practice has been explored in (Růžička et al., 2023) and in (Růžička and Markham, 2025). In the latter, different kernel sizes were used for the morphological operations. We tried all variants and report only the best performing ones. Specifically, we threshold the matched filter products by 500 ppm·m, and follow with erosion and dilation morphological operations with one of two 3x3 kernels - “ones” (all values set to ones) or “cross” (middle row and middle column full of ones).

5. Experiments

In this paper, we explore two main types of experiments. First, we explore the scenario where we have a large dataset of methane leak events and we want to select the best performing model variant. Broadly speaking, this effort will be a follow-up on the work presented by (Růžička et al., 2023), however we add several innovations to the models in terms of the used methane enhancement products, input data modalities and finally methods useful for final deployment such as model en-

sembling. Secondly, we explore the generalisation ability of the models trained in the first step with the aim to adapt the machine learning models for data from different hyperspectral sensors. Methodologically, we adapt the steps taken in the work of (Růžička and Markham, 2025), where models were pre-trained on a large dataset (in that instance of synthetic data), to be later fine-tuned and evaluated on much smaller datasets of real data. In our scenario, we adapt models pre-trained on the larger EMIT dataset to the smaller datasets of EnMAP and PRISMA sensors.

5.1. Training on EMIT datasets

Our training hyperparameters are informed by the work of (Růžička et al., 2023), our models use similar U-Net architecture, in our case with the MobileNet-v3 encoder. As inputs, we use the RGB channels of the hyperspectral data converted into reflectances alongside one of the computed methane enhancement products. In addition, we optionally provide the model with 2 additional bands of data capturing the wind information (wind direction vectors at the center location of each tile), and 3 additional bands of data encoding the location information (latitude and values of longitude represented following the approach of (Lang et al., 2023)). In our experiments, we compare which of the methane enhancement products are the best for our trained models, and if the added extra information from wind and location helps the model training.

We train these models on the EMIT dataset, which has three subsets: train, validation and test. The validation dataset is used to select the best performing checkpoint. In all experiments, we train the models for 60 epochs using the Adam optimizer

with an initial learning rate of 0.001. From our training dataset, we extract tiles of 128x128 px with an overlap of 64 px. We augment these with random rotations, spatial jitter of 16 px, and random vertical and horizontal flips to prevent the location of the methane leak events appearing in the same place during training. We use a batch size of 64 tiles. When evaluating, we process tiles in their original resolution - this is 256x256 px for the regular dataset and variable resolution of about 1280x1242 px in case of the full tile data (when needed, we pad this data with zeros to a multiple of 32).

Finally, when evaluating, we also explore model ensembles. In all experiments we repeat the training process 5 times to obtain average and standard deviation for each output. For model deployment, we make predictions using all models and then average those predictions as a final ensemble output. Each model in the ensemble uses the same architecture, but it is trained from a different random initialization and follows a stochastic training run. We also explored approaches for weight averaging, or methods to ascertain agreement between the models, but obtained worse results. While model ensembles increase the computation time needed for model inference (linearly in the number of used models), the model prediction is very fast compared to the other steps in the workflow, such as downloading the data from the NASA servers. As such, model inference does not create a computation bottleneck in the on-ground prediction scenario (as opposed to model predictions directly on satellites explored in (Růžička and Markham, 2025)).

5.2. Adaptation to PRISMA and EnMAP data

In the next set of experiments, we use the best models obtained from EMIT training, and explore how to adapt them for data from a different hyperspectral sensor. Our models use the same input modalities and due to data conversion into reflectances, the data is in similar value ranges. This makes data normalisation simpler. We also note that we can compute the same methane enhancement products from a variety of hyperspectral sensors - for that reason, we are able to use the same computed WMF product (selected as the best performing MF variant).

Our datasets from the PRISMA and EnMAP sensors are smaller and less diverse than the dataset of EMIT. For this reason, we compare (1) using models pre-trained on EMIT data in a zero-shot learning manner, with (2) training new models from scratch on the smaller datasets, and finally (3) with model fine-tuning. When fine-tuning, we can either use the data from the target sensor only (here PRISMA or EnMAP), or we can create a combined dataset from the training datasets of the EMIT and one target sensor.

When creating these smaller datasets, we chose to only split data in between train and test subsets. This enables us to use more of the data we have for training, but prevents us from selecting the best model with a validation dataset. However, we can still select the best performing models and treat the data which these models will be used with in the future as the true test datasets. Otherwise, we can always use the last checkpoint after a selected number of epochs.

Models trained from scratch use the default learning rate of 0.001 consistent with the hyperparameter settings used when training on the EMIT dataset - and are trained for 50 epochs. On the other hand, for fine-tuning models, we select a much lower learning rate of 10^{-6} and fine-tune them for 10 epochs, while evaluating at the end of each one to detect if the models are overfitting.

6. Results

In this paper, we present four main results in the following structure. Table 2 and section 6.1 explores different input modalities and their influence on the model performance. Section 6.2 further explores the evaluation of these models on full scene data and details our proposed improvements of using model ensembles to reduce false alarms. Tables 3 and 4 and section 6.3 covers adaptation between sensors. Finally, section 6.4 and 6.5 details the deployment of our models in the real production pipelines used at UNEP's IMEO.

6.1. Methane detection in EMIT data

Table 2 shows results of our baselines and proposed models comparing different input modalities, including three types of matched filter product and auxiliary data such as the wind and location information. When considering all baseline approaches, we see some variation between the different input modalities. However, all variants perform worse than any of the trained models. This is consistent with prior research and highlights the benefits that can be gained by using deep learning models for this task.

When comparing models with RGB and single methane enhancement product – the default MF, Mag1c or WMF – we observe interesting improving relation. If we focus just on the average F1 score in Table 2, the Mag1c variant performs the worst with 43.59, default MF gets 53.92, while the WMF is the best performing product with 63.07. Between the worst and the best, this is a significant score increase by over 44%. It seems that the WMF, with its improved background rejection from using a broader spectral interval, provides better target/background contrast that simplifies the learning task. Figure 6 shows the qualitative comparison between the baseline method and our proposed models.

The inclusion of auxiliary data, such as the wind and location information, further boosts the performance of our best models, however these gains are only minor in comparison with the selection of the best matched filter product. Wind information encoding boosts the average F1 score to 63.68 (improvement by just 0.61 points) and location encoding boosts this to 64.40 (improvement of additional 0.72 points). Other scores are also improved in similar magnitude.

6.2. Evaluation on full EMIT tiles

Table 2 further details evaluation of our models on the full tile test sets with the number of detected and missed methane leak events and the number of false alarms. Note that for EMIT data, we created the full tile dataset from 105 source granules

Table 2: Results on EMIT. We show the average of training 5 runs of our models.

EMIT Model variant	Tiled dataset, segmentation:				Fulltile sources, individual events:		
	AUPRC	F1	Precision	Recall	Detected	Missed	False Alarms
baseline Mag1c (thr. 500, cross)	N/A	22.45	36.22	16.27	187	124	41903
baseline MF (thr. 500, ones)	N/A	27.7	39.61	21.29	217	94	110383
baseline WMF (thr. 500, cross)	N/A	23.4	38.8	16.75	225	86	79273
U-NET RGB+Mag1c (Růžička et al., 2023)	40.87 ± 2.75	43.59 ± 3.17	53.48 ± 1.90	37.00 ± 4.36	137 ± 21	174 ± 21	5789 ± 2157
U-NET RGB+MF	56.06 ± 2.49	53.92 ± 2.14	63.04 ± 3.98	47.51 ± 4.31	203 ± 20	108 ± 20	6677 ± 2138
U-NET RGB+WMF	68.26 ± 3.06	63.07 ± 2.46	72.99 ± 1.17	55.65 ± 3.82	213 ± 20	98 ± 20	3565 ± 1830
U-NET RGB+WMF, Wind	68.97 ± 3.16	63.68 ± 2.77	69.28 ± 2.75	59.01 ± 3.69	220 ± 19	91 ± 19	5644 ± 2570
U-NET RGB+WMF, Wind, Location	69.44 ± 2.60	64.40 ± 2.08	71.88 ± 2.35	58.65 ± 4.66	191 ± 22	120 ± 21	2403 ± 899
Ensemble, 5x U-NET RGB+WMF	73.58	65.13	79.87	54.98	207	104	1501
Ensemble, 5x U-NET RGB+WMF, Wind	72.64	65.49	73.81	58.85	216	95	2118

with known plume events and 95 granules with no events. An example full tile evaluation is shown on Figure 7.

Switching from any baseline method to deep learning produces significant improvements. While the WMF baseline has over 79k false alarms, this number is reduced to just over 5.6k (using the U-Net RGB+WMF, Wind variant).

In this context we also evaluate our proposed approach of using model ensembles. This further boosts the tiled dataset statistics, achieving the best performing models in terms of scores like F1 and AUPRC. More importantly, it dramatically reduces the number of false alarms created by these models, while achieving one of the largest number of detected events (using the variant with the wind information).

We highlight that while the improvements for example over the F1 score remain relatively minor when using ensembles (by 2.84%) the main contribution is in the reduction in the number of false alerts by more than 97% over the classical baselines. This is particularly relevant for model deployment in a real production pipeline, an application which has a low tolerance for false positive errors.

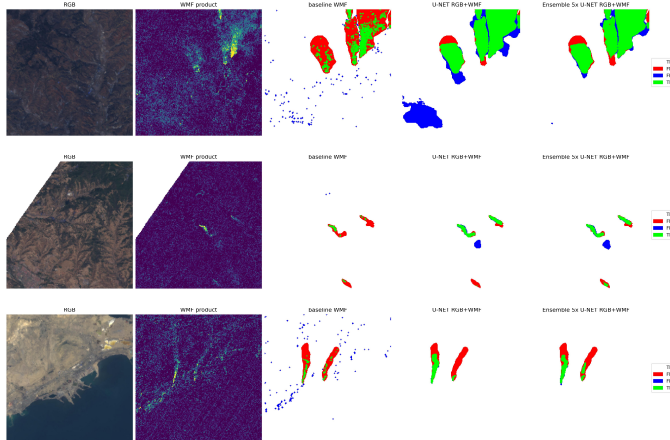


Figure 6: Qualitative results comparing our machine learning models on samples from the EMIT test dataset. Shown from left to right are predictions from the baseline (using WMF, 500 ppmxm as threshold and the “cross” kernel), single U-Net model (using RGB+WMF) and finally an ensemble of five of these models.

6.3. Adaptation to other sensors, EnMAP and PRISMA

Tables 3 and 4 present our results when evaluating model adaptation on data from EnMAP and PRISMA. In both cases, the number of methane leak events is much smaller, and as has been explored in prior research (Růžička et al., 2023; Růžička and Markham, 2025; Mancoridis et al., 2025b), zero-shot generalisation and model fine-tuning can be used to transfer knowledge learned on the larger source dataset (in our case composed of data from EMIT).

Generally, we observe relatively high zero-shot performance of the out-of-the-box models pre-trained on the EMIT data used for both EnMAP and PRISMA cases. These seem to outperform simple training from scratch approaches, which might be due to the relatively small number of methane leak events present in these additional datasets. Fine-tuning of these models usually boosts the performance further, but depending on which sensor is used, we observe different behaviour when using just the target domain, or a combination of the two datasets (source and target).

More concretely, in Table 3 we see progressive improvement in the F1 score when comparing training from scratch on EnMAP data (44.39 F1), zero-shot deployment of the EMIT model (56.84 F1) and finally fine-tuning of EMIT models on just the EnMAP data (55.32 F1), or on an extended dataset of both EMIT and EnMAP (59.28 F1). Ensembling of the best models boosts this performance to final F1 score of 64.02. In total we gain over 44% when using the ensembled fine-tuned model over model depending only on the EnMAP data, or by 12.6% when comparing against only zero-generalised EMIT model.

Here we note the importance of evaluating models on datasets with full tile samples. There, the number of detected events varies depending on the used generalisation method. Simple zero-shot generalisation of the EMIT model outperforms variants that would fine-tune only on the much smaller dataset of EnMAP images. If we instead fine-tune on a dataset constructed by combining the EMIT and EnMAP training datasets, we receive the best from the both approaches - previously discussed improvements in the F1 score and also maintained large number of detected events. We also observe reduced number of false positives. For best performance, we

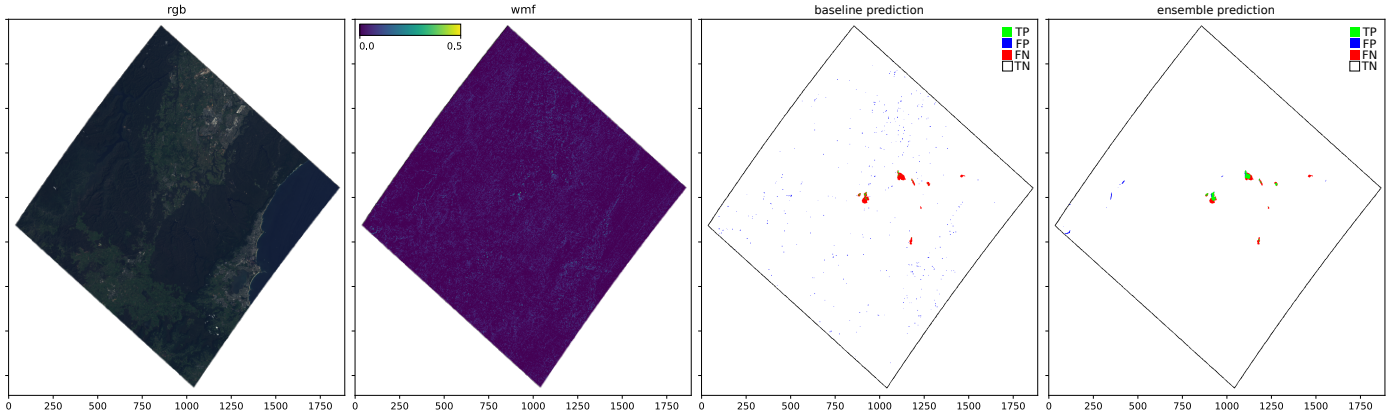


Figure 7: EMIT full tile example prediction comparing the thresholding baseline (one using WMF and the “ones” kernel) with the “Ensemble, 5x U-NET RGB+WMF, Wind” model. Note the so-called salt-and-pepper noise of the baseline, this is present even after the morphological operations. While we note that it could be further reduced by using larger kernels, true detection of real plume events would also suffer. WMF values are scaled as inputs to the model (0.5 corresponds to 4000 ppm×m). For better legibility, we recommend viewing the web version of this article.

Table 3: Results on EnMAP. We show the average of training 5 runs of our models.

EnMAP	Tiled dataset, segmentation:				Fulltile sources, individual events:		
	Model variant	AUPRC	F1	Precision	Recall	Detected	Missed
Baseline (WMF 500 thr, “ones” kernel)	N/A	35.37	37.82	33.21	116	21	20264
Train from scratch, 50 ep.	43.24 ± 3.45	44.39 ± 2.62	56.43 ± 6.91	36.85 ± 1.65	70 ± 6	67 ± 6	2132 ± 843
Zero-shot (EMIT U-NET RGB+WMF model)	62.46 ± 1.83	56.84 ± 1.57	50.61 ± 3.04	65.16 ± 3.32	103 ± 8	34 ± 8	2514 ± 1522
Fine-tune (EnMAP), 1 ep.	59.87 ± 5.84	55.32 ± 4.36	68.48 ± 4.5	46.69 ± 5.47	93 ± 7	44 ± 7	1013 ± 342
Fine-tune (EMIT+EnMAP), 4 ep.	64.49 ± 1.6	59.28 ± 1.55	55.17 ± 2.98	64.23 ± 1.97	103 ± 5	34 ± 5	1951 ± 811
Ensembled Zero-shot	68.71	61.65	58.5	65.15	102	35	1302
Ensembled Fine-tune (EMIT+EnMAP), 4 ep.	69.94	64.02	63.51	64.54	104	33	1115

can again leverage ensemble models. These reduce the number of false positives by more than 55% while maintaining the same number of detected events (comparing zero-shot against our best ensemble model). Qualitative results can be seen on example scenes in Figure 8.

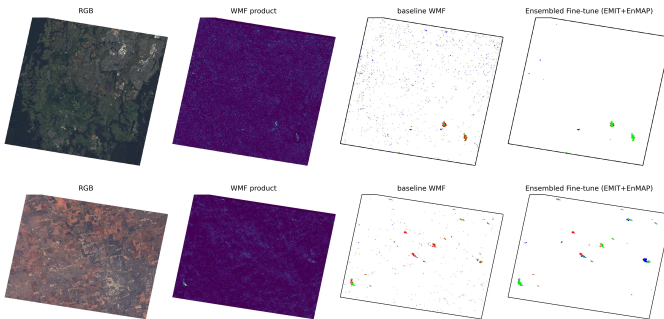


Figure 8: Model prediction examples on the EnMAP data comparing baseline approaches with our proposed Ensemble models (showing the “Ensembled Fine-tune (EMIT+EnMAP)” model).

As with the EnMAP dataset, when adapting our models for the PRISMA data in Table 4, we observe improvements in the F1 score when going from training from scratch (31.55 F1) to zero-shot deployment of the EMIT model (40.5). Finally, when fine-tuning the models on the PRISMA dataset we get a 44.37 F1 score. When fine-tuning on a dataset built from a combina-

tion of EMIT and PRISMA training datasets we get an F1 score of 42.11. There is a small difference with the EnMAP scenario, where models trained on the combined dataset had better performance, while we see slightly better performance when using the PRISMA only data. This may be due to the larger size of the available PRISMA data in contrast to the small EnMAP dataset which may lead to model overfitting when used in isolation. As before, model ensembles obtain a high F1 score (above 43), while maintaining large number of detected events and smaller number of false positive detections. Figure 9 shows an example full tile scene. Interestingly, if we wanted to use the model that detects the most events, we would chose either the model pretrained on EMIT only, or models fine-tuned on a combined dataset of PRISMA and EMIT images.

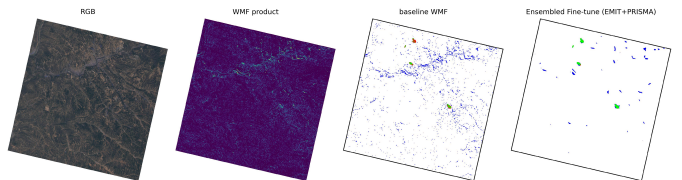


Figure 9: Model prediction examples on the PRISMA data comparing baseline approaches with our proposed Ensemble models (showing the “Ensembled Fine-tune (EMIT+PRISMA)” model).

Table 4: Results on PRISMA. We show the average of training 5 runs of our models.

PRISMA Model variant	Tiled dataset, segmentation:				Fulltile sources, individual events:		
	AUPRC	F1	Precision	Recall	Detected	Missed	False Alarms
Baseline (WMF 500 thr, “ones” kernel)	N/A	26.05	23.14	29.80	123	20	57270
Train from scratch, 50 ep.	25.91 \pm 2.52	31.55 \pm 2.56	31.0 \pm 5.32	33.61 \pm 4.94	90 \pm 16	53 \pm 16	5032 \pm 1264
Zero-shot (EMIT U-NET RGB+WMF model)	31.84 \pm 1.99	40.5 \pm 2.9	31.57 \pm 3.22	57.18 \pm 4.89	111 \pm 13	32 \pm 13	4984 \pm 2727
Fine-tune (PRISMA), 6 ep.	37.05 \pm 4.86	44.37 \pm 2.09	40.32 \pm 4.73	50.14 \pm 2.97	101 \pm 7	42 \pm 7	2806 \pm 1072
Fine-tune (EMIT+PRISMA), 2 ep.	33.0 \pm 1.25	42.11 \pm 1.16	34.36 \pm 1.77	54.71 \pm 3.35	107 \pm 8	36 \pm 8	3715 \pm 1665
Ensembled Zero-shot	35.6	44.04	37.02	54.36	113	30	2881
Ensembled Fine-tune (PRISMA), 6 ep.	40.61	43.61	43.11	44.13	103	40	1674
Ensembled Fine-tune (EMIT+PRISMA), 2 ep.	36.08	43.79	37.97	51.72	106	37	2248

6.4. Results from operational deployment

Table 5: Operational deployment results. The numbers correspond to the statistics in early November 2025 after 7 months of model deployment. As this is a living system, these numbers increase daily.

	EMIT	EnMAP	PRISMA
Processed tiles	11,693	6,774	1,100
Verified detected plumes	1,059	222	70
Different countries	54	26	14
Plumes notified	395	56	28

Table 5 presents the results of using our proposed models in the operational detection pipeline used at the Methane Alert and Response System (MARS) at the United Nations Environmental Program (UNEP).

Internally within the UNEP’s IMEO, a tool called Plume Viewer is used to collect information from multiple sensors over areas informed by previously known emission locations and vector maps of relevant assets. There, a team of analysts searches through daily monitoring data and manually delineates and verifies the methane leak events. Needless to say, this process is quite labour intensive and can tremendously benefit from even semi-automated detection tools. For that purpose, our models were developed to perform semantic segmentation as a pre-processing step that aids with this manual search process. Figure 11 shows the interface and examples of methane leak events proposed by our models to the human reviewers. Despite producing false positive detections, the models remain useful in guiding the reviewers towards potential methane leak events in the scene. During their review, the analyst marks the correctly detected plumes as validated (either using the model suggested boundary, or by drawing a new one as a vector) and then with one click deletes all non-validated detections. The validated detections then undergo an internal review process and are eventually notified to the relevant operators and governmental actors.

This operational workflow is similar to the one used in (Vaughan et al., 2024b), but rather than just predicting on selected a priori known monitoring locations, we run our models on the full scenes captured by the satellite. This allows us to discover new regions of interest and to expand the map of tracked

monitoring sites. For further automation, the information about the proximity of known emitters can also be used, for example by using different thresholds for model prediction in these areas. Using our models for full scene predictions is possible thanks to the insights from section 6.2.

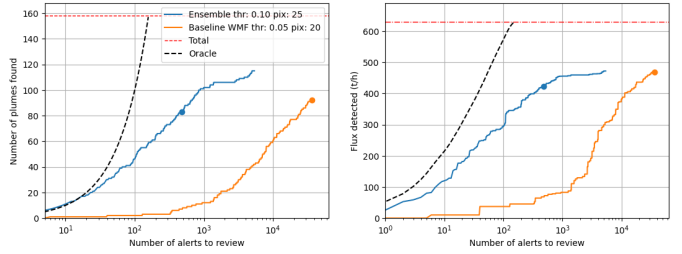


Figure 10: Deployed sorting performance using our models on events between February and September 2025 (from EMIT, PRISMA and EnMAP). Note that these are not included in our created test sets, they correspond to the new data processed throughout the operational use of our model. We show two different approaches to sorting our model predictions and highlight how many events are detected after reviewing an increasing proportion of all predicted plumes (alerts). Please note that this analysis considers only plumes from fully validated scenes, as such the number does not match the number of verified detected plumes in Table 5 (an analyst can mark a single model prediction as verified without validating the full scene).

Figure 10 demonstrates performance of our models for plumes between February and September 2025. In this scenario we sort plume predictions by their assigned score. In order to compute this score we first use an initial threshold of 0.1 to delineate individual plume predictions. Afterwards, we calculate the plume score as the minimum threshold of the probability map such that there are at least $N=25$ connected pixels inside the delineated plume (parameters for the best performing baseline are the initial threshold of 0.05 and $N=20$). In the figure of the left, we show on the x-axis the number of plumes that needs to be analysed in order to catch the number of plumes on the y-axis. The Oracle marks the 1:1 line (shown in log), where each analysed prediction is a true plume - this is the upper bound given a perfect knowledge. On the figure of the right we show on the y-axis the total flux of the captured plumes. We use IME method (Frankenberg et al., 2016; Varon et al., 2018) to compute the flux rate. Model plume scores mostly consider the morphology of each plume, quantifications the estimated intensity, while scores proposed by the recent (Xiang et al., 2025)

consider the spectral match with the known target signature of methane - these three likely contain complementary information.

Notably, we first deployed models for detecting methane leaks in the EMIT data, and later the fine-tuned model variants for EnMAP and PRISMA data. We currently leverage the best performing model ensembles in the detection pipelines. Due to the higher cadence of observations produced by EMIT, the number of processed tiles listed in Table 5 is higher.

6.5. Mitigation cases

In Figure 12, we showcase several detections over four cases where MARS notifications triggered successful mitigation actions¹. These examples demonstrate the operational use of the model to sift through the large amount of EMIT data, not only to detect potential methane plumes, but also to confirm if mitigation actions stopped the leaks. Figure 12, from top to bottom, shows the detection results for mitigation cases in Libya, Argentina, Oman, and Azerbaijan before and after the undertaken actions. In Libya, using the newly deployed AI model in production, emissions at the Zaggut Station in the Waha Oil Field were detected when the wind extinguished a flare. The operator reignited it on June 6th, 2025, ending the release. In Argentina, plumes detected in March 2023 over a facility in Neuquén province prompted rapid repairs following notification. In Oman, emissions were observed on February 2nd, 2025, in the Northwest Oman and Jahlah North areas. The emissions were traced to a faulty valve and leaking flowline, both repaired within 48 hours after receiving the notification. In Azerbaijan, imagery from July–August 2024 revealed several plumes over the Neft Daşları offshore complex, after which the operator installed low-pressure gas lines to recover vented gas from two of the identified sources in a few weeks and committed to work in mitigation activities to fix the remaining notified sources in the following months. Both detections and non-detections in Fig. 12 are consistent with feedback received by the MARS team, highlighting the value of AI-based monitoring not only for the discovery of new leaks, but also for confirming emission-free conditions and identifying potential successful mitigation interventions.

7. Discussion and Conclusion

This paper detailed the operational deployment of a machine learning system for detecting methane plumes across three imaging spectroscopy instruments: EMIT, PRISMA and EnMAP. This work was made possible by our creation of the largest publicly available dataset of manually annotated methane plumes from these sensors. We have released this dataset to the research community to serve as a benchmark and to accelerate the development of future AI models in this critical domain (<https://huggingface.co/datasets/UNEP-IMEO/MARS-Hyperspectral>).

¹These cases are listed as the MARS Mitigation Case Studies: <https://www.unep.org/topics/energy/methane/mars-case-studies>

Our results demonstrate that the choice of input product can significantly impact the AI model performance. Through a quantitative comparison, we found that models using the wide-window matched filter (Roger et al., 2023) as input achieve substantially higher F1 scores (63.07 ± 2.56) than those using either Mag1c (Foote et al., 2020b) (43.59 ± 3.17) or the standard matched filter (53.92 ± 2.14) (Table 2). Furthermore, our ensemble models outperformed non-machine learning baselines by a significant margin, increasing the F1 score between 135% to 191% on the tiled test dataset (Tables 2, 3 and 4).

A key finding of our study is the model’s strong cross-sensor generalization. Models trained on EMIT data achieved robust zero-shot performance on both PRISMA and EnMAP datasets, a capability further enhanced through fine-tuning (Tables 3 and 4). This successful application of transfer learning is significant as it demonstrates that a model trained on a large, high-quality dataset from a source mission like EMIT can be rapidly deployed for new sensors with similar observational characteristics, accelerating their operational readiness.

An important lesson learned from the operational deployment is the necessity of evaluating models on full satellite granules which exposes performance issues not apparent in tiled datasets. While our initial models produced numerous false positives on these full scenes, we found that model ensembles provided a simple yet effective approach, to reducing false positive detections by over 74% (in comparison with previous deep learning models presented in (Růžička et al., 2023)). This issue stems from the out-of-distribution (OOD) challenge inherent within our application; the training data is necessarily biased toward locations with methane-emitting infrastructure. Consequently, when a model processes a full granule, it encounters vast areas of OOD content—such as cities, roads, rivers, and mountains—that were underrepresented during training. Ensembling mitigates this problem by smoothing over-confident predictions on unfamiliar terrains and the resulting model uncertainty can be used to identify these OOD samples automatically (Beluch et al., 2018; Gal and Ghahramani, 2016; Růžička et al., 2020). This finding suggests that, in addition to ensembling, future work should focus on curating a more exhaustive set of negative training samples to further improve model robustness.

Our models have been successfully integrated into the operational workflow of the MARS at UNEP’s IMEO. Over approximately 5 months of deployment, the system has facilitated the verification of 1,351 methane leak event, leading to 479 formal stakeholder notifications and 1 machine learning driven methane leak mitigation. Crucially, the system enables the discovery of previously unknown emission sources by systematically monitoring coverage of MARS and enhances the comprehensiveness of global methane emission observations.

Looking ahead, we identify two promising research directions for further reducing false positive detections. One approach is to implement a post-processing filter based on the spectral similarity of model-delineated plumes, a technique explored in (Xiang et al., 2025). A more fundamental alternative involves developing end-to-end machine learning models that learn directly from radiance data (Růžička and Markham,

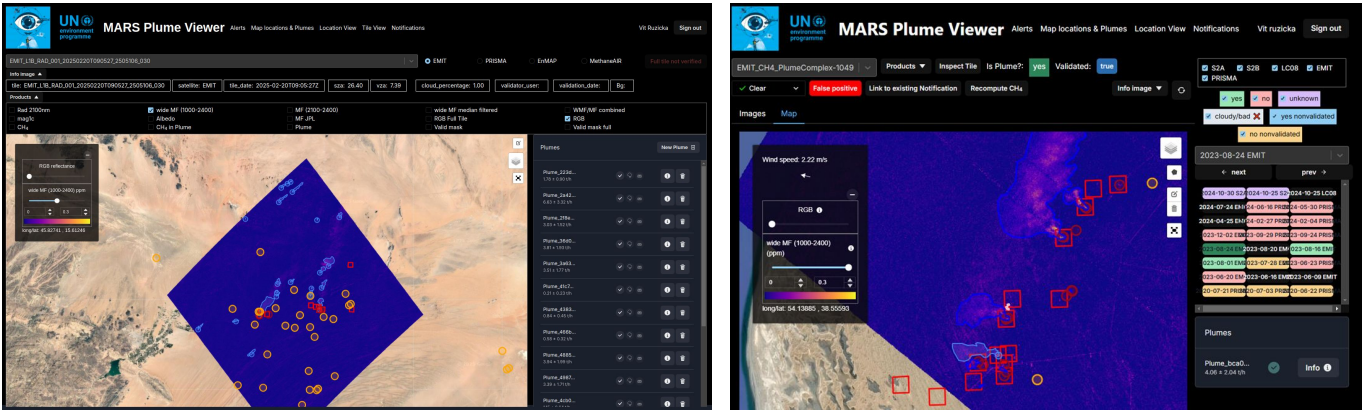


Figure 11: Example of the PlumeViewer interface used to search for methane leak events. Our models were integrated and the vectorized model prediction (in light blue) is shown for two example EMIT images. The scene on the left has not yet been manually cleaned from the false alarms, this is to demonstrate the usefulness of the system even in scenarios with false positive detections. The red squares are made around monitoring locations - these are drawn around verified plume events to help inform detections of future satellite captures.

2025). Such an approach could yield significant performance gains by bypassing the reliance on intermediate methane enhancement products, which can introduce noise and limit accuracy. Another promising research direction is the integration of diverse, expert-annotated datasets to create more nuanced ground truth labels. Combining the labels from this work with those recently released by (Green et al., 2023), for instance, would enable a systematic analysis of inter-expert agreement. This approach mirrors advances in other remote sensing fields, such as cloud segmentation, where multi-class labels have proven superior to simple binary masks (Aybar et al., 2022). For methane detection, such refined labels would be invaluable, allowing models to differentiate between strong and weak emissions to characterize plume morphology by distinguishing the dense source from its more diffuse tail.

It is crucial to recognize that our models and datasets are part of a living system, continuously updated with newly discovered and labeled events. This operational context, with its daily influx of data, makes it an ideal candidate for advanced machine learning paradigms. Methodologies from the Never Ending Learning (NEL) literature (Mitchell et al., 2018), Deep Active Learning (AL) (Růžička et al., 2020), or Continual Learning (CL) (Wang et al., 2024) could be very beneficial for ensuring the system’s lifelong, iterative improvement and sustained accuracy and robustness.

In conclusion, the strong generalization capabilities of our models across multiple high spatial resolution imaging spectroscopy missions highlight their immediate and future utility. While performance can be enhanced through fine-tuning or advanced techniques like generative style transfer between instruments (Mancoridis et al., 2025a), the robust zero-shot performance observed in our study is particularly significant. This capability is critical for the rapid, effective analysis from new and upcoming satellite missions, paving the way for a truly global, responsive, and AI-driven methane monitoring system—a critical tool for enabling targeted mitigation actions and addressing a key driver of near-term climate change.

8. Acknowledgements

We would like to thank the analysts of MARS UNEP IMEO for their valuable contributions in identifying methane plumes. In addition to the authors of this paper, we gratefully acknowledge the efforts of Carol Castaneda, Alma Raunak, Marc Watine, and Adriana Valverde. We acknowledge the rest of the MARS team Meghan Demeter, Tharwat Mokalled, Giulia Bonazzi, Florencia Carreras, Konstantin Kosumov and Queen Safari, for their work in country engagement and in the notification process. A portion of this work was carried out at the Jet Propulsion Laboratory, California Institute of Technology, under a contract with the National Aeronautics and Space Administration (80NM0018D0004). Part of Vít Růžička’s research was supported by an appointment to the NASA Postdoctoral Program at the Jet Propulsion Laboratory, administered by Oak Ridge Associated Universities under contract with NASA.

References

Cesar Aybar, Luis Ysuhuaylas, Jhomira Loja, Karen Gonzales, Fernando Herrera, Lesly Bautista, Roy Yali, Angie Flores, Lissette Diaz, Nicole Cuena, et al. Cloudsen12, a global dataset for semantic understanding of cloud and cloud shadow in sentinel-2. *Scientific data*, 9(1):782, 2022. 12

William H Beluch, Tim Genewein, Andreas Nürnberger, and Jan M Köhler. The power of ensembles for active learning in image classification. In *Proceedings of the IEEE conference on computer vision and pattern recognition*, pages 9368–9377, 2018. 5, 11

L.R. Brown, K. Sung, D.C. Benner, V.M. Devi, V. Boudon, T. Gabard, C. Wenger, A. Campargue, O. Leshchishina, S. Kassi, D. Mondelain, L. Wang, L. Daumont, L. Régalaia, M. Rey, X. Thomas, Vl. G. Tyuterev, O.M. Lyulin, A.V. Nikitin, H.M. Niederer, S. Albert, S. Bauerecker, M. Quack, J.J. O’Brien, I.E. Gordon, L.S. Rothman, H. Sasada, A. Coustenis, M.A.H. Smith, T. Carrington, X.-G. Wang, A.W. Mantz, and P.T. Spickler. Methane line parameters in the hitran2012 database. *Journal of Quantitative Spectroscopy and Radiative Transfer*, 130:201–219, 2013. ISSN 0022-4073. doi: <https://doi.org/10.1016/j.jqsrt.2013.06.020>. URL <https://www.sciencedirect.com/science/article/pii/S0022407313002744>. HITRAN2012 special issue. 5

Brian D Bue, Jake H Lee, Andrew K Thorpe, Philip G Brodrick, Daniel Cusworth, Alana Ayasse, Vassiliki Mancoridis, Anagha Satish, Shujun Xiong, and Riley Duren. Towards operational automated greenhouse gas plume detection. *arXiv preprint arXiv:2505.21806*, 2025. 2, 3

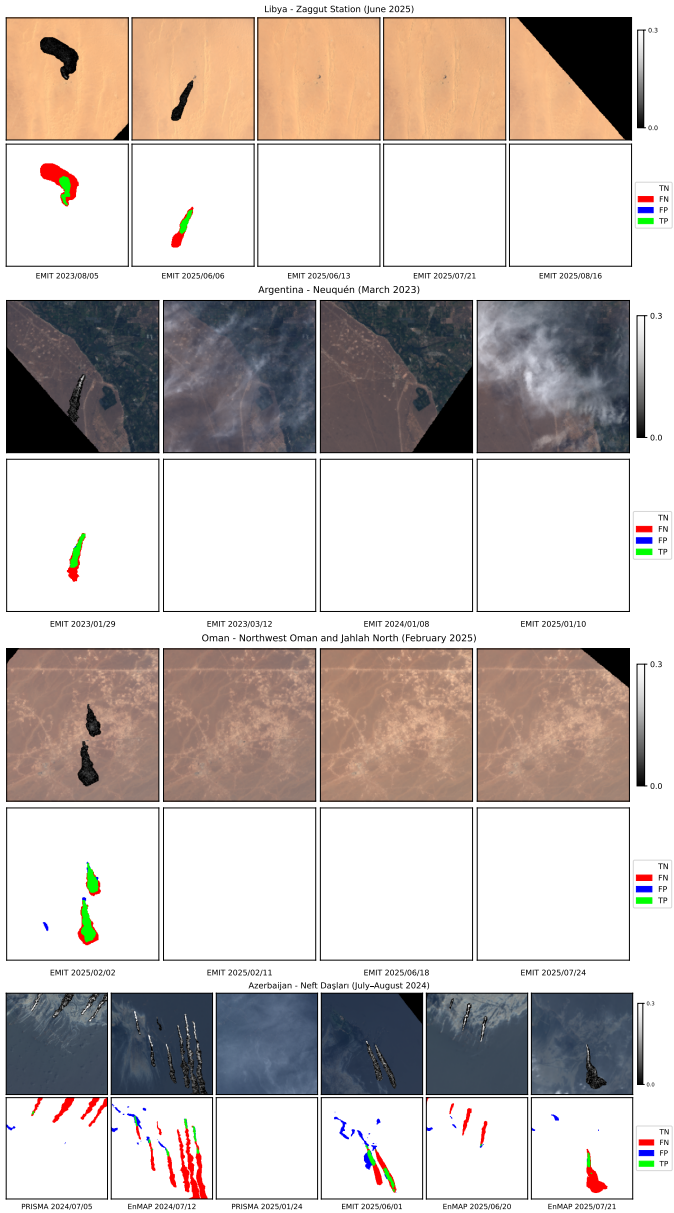


Figure 12: Mitigation case studies showing a time series of images from a selection of hyperspectral satellites with predictions of our models compared with the delineated ground truth masks. In the first row, we show an example mitigation case where our machine learning models were already operationally deployed, and aided in the notification process. In these examples, UNEP has sent MARS notifications to the relevant operators which has lead to fixing of problems that caused these leaks. The last row presents a multi-sensor example, where some parts of the overall infrastructure were fixed, while other segments were scheduled for a more concrete fix in the future. The system presented in this paper can both detect new methane emissions, but it can also be used to help with estimations of the consistency of these mitigation cases.

Sergio Cogliati, F Sarti, Leandro Chiarantini, M Cosi, R Lorusso, Ettore Lopinto, Franco Miglietta, Lorenzo Genesio, Luis Guanter, Alexander Damm, et al. The prisma imaging spectroscopy mission: overview and first performance analysis. *Remote sensing of environment*, 262:112499, 2021. 3

Daniel H Cusworth, Riley M Duren, Andrew K Thorpe, Winston Olson-Duvall, Joseph Heckler, John W Chapman, Michael L Eastwood, Mark C Helminger, Robert O Green, Gregory P Asner, et al. Intermittency of large methane emitters in the permian basin. *Environmental Science & Technology Letters*, 8(7):567–573, 2021. 2

Riley M Duren, Andrew K Thorpe, Kelsey T Foster, Talha Rafiq, Francesca M

Hopkins, Vineet Yadav, Brian D Bue, David R Thompson, Stephen Conley, Nadia K Colombi, et al. California’s methane super-emitters. *Nature*, 575 (7781):180–184, 2019. 2

Markus D Foote, Philip E Dennison, Andrew K Thorpe, David R Thompson, Siraput Jongaramrunguang, Christian Frankenberg, and Sarang C Joshi. Fast and accurate retrieval of methane concentration from imaging spectrometer data using sparsity prior. *IEEE Transactions on Geoscience and Remote Sensing*, 58(9):6480–6492, 2020a. 5

Markus D. Foote, Philip E. Dennison, Andrew K. Thorpe, David R. Thompson, Siraput Jongaramrunguang, Christian Frankenberg, and Sarang C. Joshi. Fast and Accurate Retrieval of Methane Concentration From Imaging Spectrometer Data Using Sparsity Prior. *IEEE Transactions on Geoscience and Remote Sensing*, 58(9):6480–6492, September 2020b. ISSN 1558-0644. doi: 10.1109/TGRS.2020.2976888. Conference Name: IEEE Transactions on Geoscience and Remote Sensing. 2, 11

Christian Frankenberg, Andrew K Thorpe, David R Thompson, Glynn Hulley, Eric Adam Kort, Nick Vance, Jakob Borchardt, Thomas Krings, Konstantin Gerlowski, Colm Sweeney, et al. Airborne methane remote measurements reveal heavy-tail flux distribution in four corners region. *Proceedings of the national academy of sciences*, 113(35):9734–9739, 2016. 2, 10

Yarin Gal and Zoubin Ghahramani. Dropout as a bayesian approximation: Representing model uncertainty in deep learning. In *international conference on machine learning*, pages 1050–1059. PMLR, 2016. 11

Javier Gorroño, Daniel J Varon, Itziar Irakuliz-Loitxate, and Luis Guanter. Understanding the potential of sentinel-2 for monitoring methane point emissions. *Atmospheric Measurement Techniques*, 16(1):89–107, 2023. 1

R. Green. EMIT L1B At-Sensor Calibrated Radiance and Geolocation Data 60 m V001. Distributed by NASA EOSDIS Land Processes Distributed Active Archive Center, 2022. URL <https://doi.org/10.5067/EMIT/EMITL1BRAD.001>. Accessed 2024-09-29. 3

R. Green, A. Thorpe, P. Brodrick, D. Chadwick, A. Lopez, C. Elder, C. Villanueva-Weeks, J. Fahlen, R. W. Coleman, D. Jensen, H. Bender, Q. Vinckier, C. Xiang, W. Olson-Duvall, S. Lundein, and D. Thompson. EMIT L2B Estimated Methane Plume Complexes 60 m V001. NASA Land Processes Distributed Active Archive Center., 2023. URL <https://doi.org/10.5067/EMIT/EMITL2BCH4PLM.001>. Accessed 2025-08-12. 12

Alexis Groschenry, Clement Giron, Thomas Lauvaux, Alexandre d’Aspremont, and Thibaud Ehret. Detecting methane plumes using prisma: Deep learning model and data augmentation. *arXiv preprint arXiv:2211.15429*, 2022. 2

Luis Guanter, Itziar Irakuliz-Loitxate, Javier Gorroño, Elena Sánchez-García, Daniel H Cusworth, Daniel J Varon, Sergio Cogliati, and Roberto Colombo. Mapping methane point emissions with the prisma spaceborne imaging spectrometer. *Remote Sensing of Environment*, 265:112671, 2021. 1, 2

Andrew Howard, Mark Sandler, Grace Chu, Liang-Chieh Chen, Bo Chen, Mingxing Tan, Weijun Wang, Yukun Zhu, Ruoming Pang, Vijay Vasudevan, et al. Searching for mobilenetv3. In *Proceedings of the IEEE/CVF international conference on computer vision*, pages 1314–1324, 2019. 5

Itziar Irakuliz-Loitxate, Luis Guanter, Yin-Nian Liu, Daniel J Varon, Joannes D Maasakkers, Yuzhong Zhang, Apisada Chulakadabba, Steven C Wofsy, Andrew K Thorpe, Riley M Duren, et al. Satellite-based survey of extreme methane emissions in the permian basin. *Science Advances*, 7(27):eabf4507, 2021. 2

Itziar Irakuliz-Loitxate, Luis Guanter, Joannes D Maasakkers, Daniel Zavala-Araiza, and Ilse Aben. Satellites detect abatable super-emissions in one of the world’s largest methane hotspot regions. *Environmental science & technology*, 56(4):2143–2152, 2022. 1, 2

Siraput Jongaramrunguang, Andrew K Thorpe, Georgios Matheou, and Christian Frankenberg. Methanet—an ai-driven approach to quantifying methane point-source emission from high-resolution 2-d plume imagery. *Remote Sensing of Environment*, 269:112809, 2022. 2

Peter Joyce, Cristina Ruiz Villena, Yahui Huang, Alex Webb, Manuel Gloor, Fabien H Wagner, Martyn P Chipperfield, Rocío Barrio Guilló, Chris Wilson, and Hartmut Boesch. Using a deep neural network to detect methane point sources and quantify emissions from prisma hyperspectral satellite images. *Atmospheric Measurement Techniques*, 16(10):2627–2640, 2023. 2

Satish Kumar, Ivan Arevalo, ASM Iftekhar, and BS Manjunath. Methanemap: Spectral absorption aware hyperspectral transformer for methane detection. In *Proceedings of the IEEE/CVF Conference on Computer Vision and Pattern Recognition*, pages 17609–17618, 2023. 2

Johan CI Kuylensierna, Eleni Michalopoulou, and Chris Malley. Global

methane assessment: Benefits and costs of mitigating methane emissions, 2021. 1

Nico Lang, Walter Jetz, Konrad Schindler, and Jan Dirk Wegner. A high-resolution canopy height model of the earth. *Nature Ecology & Evolution*, 7(11):1778–1789, 2023. 5, 6

Hoesung Lee, Katherine Calvin, Dipak Dasgupta, Gerhard Krinner, Aditi Mukherji, Peter Thorne, Christopher Trisos, José Romero, Paulina Aldunce, Ko Barret, et al. Ipcc, 2023: Climate change 2023: Synthesis report, summary for policymakers. contribution of working groups i, ii and iii to the sixth assessment report of the intergovernmental panel on climate change [core writing team, h. lee and j. romero (eds.)]. ipcc, geneva, switzerland. 2023. 1

Vassiliki Mancoridis, Brian Bue, Jake H Lee, Andrew K Thorpe, Daniel Cusworth, Alana Ayasse, Philip G Brodrick, and Riley Duren. Multi-platform methane plume detection via model and domain adaptation. *arXiv preprint arXiv:2506.06348*, 2025a. 12

Vassiliki Mancoridis, Brian Bue, Jake H Lee, Andrew K Thorpe, Daniel Cusworth, Alana Ayasse, Philip G Brodrick, and Riley Duren. Multi-platform methane plume detection via model and domain adaptation. *arXiv preprint arXiv:2506.06348*, 2025b. 2, 8

Tom Mitchell, William Cohen, Estevam Hruschka, Partha Talukdar, Bishan Yang, Justin Betteridge, Andrew Carlson, Bhavana Dalvi, Matt Gardner, Bryan Kisiel, et al. Never-ending learning. *Communications of the ACM*, 61(5):103–115, 2018. 12

Andrea Molod, Lawrence Takacs, Max Suarez, Julio Bacmeister, In-Sun Song, and Andrew Eichmann. The geos-5 atmospheric general circulation model: Mean climate and development from merra to fortuna. Technical report, NASA, Goddard Space Flight Center, Greenbelt, Maryland, USA, 2012. 4

Javier Roger, Luis Guanter, Javier Gorroño, and Itziar Irakulis-Loitxate. Exploiting the entire near-infrared spectral range to improve the detection of methane plumes with high-resolution imaging spectrometers. *Atmospheric Measurement Techniques Discussions*, 2023:1–21, 2023. 2, 5, 11

Javier Roger, Itziar Irakulis-Loitxate, Adriana Valverde, Javier Gorroño, Sabine Chabrillat, Maximilian Brell, and Luis Guanter. High-resolution methane mapping with the enmap satellite imaging spectroscopy mission. *IEEE Transactions on Geoscience and Remote Sensing*, 62:1–12, 2024. 1, 2

Olaf Ronneberger, Philipp Fischer, and Thomas Brox. U-net: Convolutional networks for biomedical image segmentation. In *International Conference on Medical image computing and computer-assisted intervention*, pages 234–241. Springer, 2015. 5

Vít Růžička. *Intelligent decision making on-board satellites*. PhD thesis, University of Oxford, 2025. 2, 5

Vít Růžička and Andrew Markham. HyperspectralViTs: General hyperspectral models for on-board remote sensing. *IEEE Journal of Selected Topics in Applied Earth Observations and Remote Sensing*, 18:10241–10253, 2025. doi: 10.1109/JSTARS.2025.3557527. 2, 6, 7, 8, 11

Vít Růžička, Stefano D’Aronco, Jan Dirk Wegner, and Konrad Schindler. Deep active learning in remote sensing for data efficient change detection. *arXiv preprint arXiv:2008.11201*, 2020. 5, 11, 12

Vít Růžička, Gonzalo Mateo-García, Luis Gómez-Chova, Anna Vaughan, Luis Guanter, and Andrew Markham. Semantic segmentation of methane plumes with hyperspectral machine learning models. *Scientific Reports*, 13(1):19999, 2023. 2, 3, 5, 6, 8, 11

Elena Sánchez-García, Javier Gorroño, Itziar Irakulis-Loitxate, Daniel J Varon, and Luis Guanter. Mapping methane plumes at very high spatial resolution with the worldview-3 satellite. *Atmospheric Measurement Techniques Discussions*, 2021:1–26, 2021. 2

Tobias Storch, Hans-Peter Honold, Sabine Chabrillat, Martin Habermeyer, Paul Tucker, Maximilian Brell, Andreas Ohndorf, Katrin Wirth, Matthias Betz, Michael Kuchler, Helmut Mühle, Emiliano Carmona, Simon Baur, Martin Mücke, Sebastian Löw, Daniel Schulze, Steffen Zimmermann, Christoph Lenzen, Sebastian Wiesner, Saika Aida, Ralph Kahle, Peter Willburger, Sebastian Hartung, Daniele Dietrich, Nicolae Plesia, Mirco Tegler, Katharina Schork, Kevin Alonso, David Marshall, Birgit Gerasch, Peter Schwind, Miguel Pato, Mathias Schneider, Raquel de los Reyes, Maximilian Langheinrich, Julian Wenzel, Martin Bachmann, Stefanie Holzwarth, Nicole Pinell, Luis Guanter, Karl Segl, Daniel Scheffler, Saskia Foerster, Niklas Bohn, Astrid Bracher, Mariana A. Soppa, Ferran Gascon, Rob Green, Raymond Kokaly, Jose Moreno, Cindy Ong, Manuela Sornig, Ricarda Wernitz, Klaus Bagschik, Detlef Reintsema, Laura La Porta, Anke Schickling, and Sebastian Fischer. The enmap imaging spectroscopy mission towards operations. *Remote Sensing of Environment*, 294:113632, 2023. ISSN 0034-4257. doi: <https://doi.org/10.1016/j.rse.2023.113632>. URL <https://www.sciencedirect.com/science/article/pii/S0034425723001839>. 3

D. R. Thompson and P. G. Brodrick. Realizing machine learning’s promise in geoscience remote sensing. *EOS*, 102, July 2021. doi: 10.1029/2021EO160605. 2

DR Thompson, I Leifer, H Bovensmann, M Eastwood, M Fladeland, C Frankenberg, K Gerilowski, RO Green, S Kratwurst, T Krings, et al. Real-time remote detection and measurement for airborne imaging spectroscopy: a case study with methane. *Atmospheric Measurement Techniques*, 8(10):4383–4397, 2015. 2

DR Thompson, AK Thorpe, C Frankenberg, RO Green, R Duren, Luis Guanter, Andre Hollstein, E Middleton, L Ong, and S Ungar. Space-based remote imaging spectroscopy of the also canyon ch4 superemitter. *Geophysical Research Letters*, 43(12):6571–6578, 2016. 2

Enno Tiemann, Shanyu Zhou, Alexander Kläser, Konrad Heidler, Rochelle Schneider, and Xiao Xiang Zhu. Machine learning for methane detection and quantification from space—a survey. *arXiv preprint arXiv:2408.15122*, 2024. 2

UNEP United Nations Environment Programme. An eye on methane 2024, 2024. URL <https://www.unep.org/resources/eye-methane-2024>. 2

Daniel J Varon, Daniel J Jacob, Jason McKeever, Dylan Jervis, Berke OA Durak, Yan Xia, and Yi Huang. Quantifying methane point sources from fine-scale satellite observations of atmospheric methane plumes. *Atmospheric Measurement Techniques*, 11(10):5673–5686, 2018. 10

Daniel J Varon, Dylan Jervis, Jason McKeever, Ian Spence, David Gains, and Daniel J Jacob. High-frequency monitoring of anomalous methane point sources with multispectral sentinel-2 satellite observations. *Atmospheric Measurement Techniques Discussions*, 2020:1–21, 2020. 1, 2

Anna Vaughan, Gonzalo Mateo-García, Luis Gómez-Chova, Vít Růžička, Luis Guanter, and Itziar Irakulis-Loitxate. Ch4net: a deep learning model for monitoring methane super-emitters with sentinel-2 imagery. *EGUspHERE*, 2023:1–17, 2023. 3

Anna Vaughan, Gonzalo Mateo-García, Itziar Irakulis-Loitxate, Marc Watine, Pablo Fernandez-Poblan, Richard E Turner, James Requeima, Javier Gorroño, Cynthia Randles, Manfredi Caltagirone, et al. Ai for operational methane emitter monitoring from space. *arXiv preprint arXiv:2408.04745*, 2024a. 5

Anna Vaughan, Gonzalo Mateo-García, Itziar Irakulis-Loitxate, Marc Watine, Pablo Fernandez-Poblan, Richard E Turner, James Requeima, Javier Gorroño, Cynthia Randles, Manfredi Caltagirone, et al. Ai for operational methane emitter monitoring from space. *arXiv preprint arXiv:2408.04745*, 2024b. 3, 10

Liyuan Wang, Xingxing Zhang, Hang Su, and Jun Zhu. A comprehensive survey of continual learning: Theory, method and application. *IEEE Transactions on Pattern Analysis and Machine Intelligence*, 46(8):5362–5383, 2024. doi: 10.1109/TPAMI.2024.3367329. 12

Chuchu Xiang, David R Thompson, Robert O Green, Jay E Fahlen, Andrew K Thorpe, Philip G Brodrick, Red Willow Coleman, Amanda M Lopez, and Clayton D Elder. Identification of false methane plumes for orbital imaging spectrometers: A case study with emit. *Remote Sensing of Environment*, 328:114860, 2025. 10, 11